Neutral Depletion in a Collisionless Plasma

Amnon Fruchtman, *Member, IEEE*

***Abstract*—Neutral depletion can significantly affect the steady state of low-temperature plasmas. Recent theoretical analyses predicted unexpected effects of neutral depletion in both collisional and collisionless regimes. In this paper, we address the effects of neutral depletion on the steady state of a collisionless plasma generated in a collisionless neutral gas. The neutrals and the plasma are coupled only through volume ionization and wall recombination. For a closed system with zero mass flow, the density profiles of both plasma and neutrals are found, and values for the rate of depletion at asymptotic limits are derived. It is shown that the pressure of the collisionless neutral gas is maximal where the density is minimal. This is in contrast to the case in which the neutral gas is thermalized. For an open system of a nonzero mass flow, analytical expressions are derived for the profiles of the plasma and the neutral flows. Considering such a configuration for a plasma thruster, we calculate the expected thrust, propellant utilization, specific impulse, and efficiency. The energy cost for ionization and backwall energy losses are shown to significantly reduce the efficiency.**

***Index Terms*—Ballistic neutrals, collisionless ions, gas discharges, neutral depletion, plasma thrusters.**

I. Introduction

SPACE and laboratory plasmas can be significantly affected by neutral depletion. The effect of neutral depletion in gas discharges has already been addressed in some early insightful studies [1]–[5]. However, only in recent years, with the growing use of lower pressure and higher power radio-frequency discharges, is the importance of neutral depletion becoming fully recognized [6]–[21]. The decrease of the neutral density [6]–[8], [11], [14], [16], [18]–[21], relaxation oscillations [9], [10], and neutral-gas heating [12], [13], [15], [17], [21] have been measured. In weakly ionized plasmas, in which the neutral density and temperature are uniform, particle balance is decoupled from power balance, and the electron temperature is found to be related to a single similarity variable, which is the product of the neutral-gas pressure and the plasma spatial extent (the Paschen parameter) [22]–[28]. The plasma density is determined by power balance and monotonically increases with deposited energy, as does the plasma flux. When ionization is intense and neutral depletion is significant, so that neutral pressure is not uniform, the aforementioned similarity variable is no longer well defined. Moreover, particle and power balances become coupled and so do ionization and transport.

Recent theoretical studies focused on the effect of neutral depletion on the steady state of low-temperature plasmas [29]–[33]. In these studies, the total number of neutrals has been found to replace the Paschen parameter as the similarity variable that determines the electron temperature. Neutral depletion in a collisional plasma that is in pressure balance with the neutral gas has been studied in [29], and the enhancement of the depletion due to neutral-gas heating by collisions with plasma electrons has been analyzed in [33]. It has been shown in [29] that, because of the inherent coupling of ionization and transport, an increase of the energy invested in ionization can nonlinearly enhance the transport process. Such an enhancement of the plasma transport due to neutral depletion was shown to result in an unexpected decrease of the plasma density when power is increased, despite the increase of the flux of generated plasma. An unexpected feature of the steady state has also been found for collisionless plasma due to strong ionization [32]. For collisionless neutral gas, the strong ionization resulted in an expected neutral-gas-density minimum at the center of the chamber [30], [31], which is called a neutral depletion. However, if the neutral gas is thermalized, that strong ionization results in a maximum of the neutral-gas density that is surprisingly located at the center of the chamber [32], which could be called neutral repletion.

In this paper, we extend the analyses that have been presented in recent conferences [30], [31], in which the neutral gas was assumed collisionless. The neutrals are assumed to move ballistically and, contrary to the case in [29], do not exchange momentum with the plasmas; rather, they interact with the plasma only through volume ionization and wall recombination. Moreover, the neutrals here are not thermalized, in contrast to [32], where they were assumed to be thermalized, although, there also, they were assumed not to exchange momentum with the plasma. The dynamics of neutrals under the assumptions in this paper has been described in a somewhat similar manner in other studies [2]–[5], [14], [16]. In this paper, we analyze both a closed system with a zero mass flow and an open system with a finite mass flow. We found that the closed system with zero mass flow, an analysis of which we presented in [31], has actually been analyzed in the past in [2]. Our analysis here provides the explanation for the contrast between the neutral profile types, depletion and repletion, which we previously mentioned. As shown here, it is the relation between the neutral density and pressure that determines whether there will be depletion or repletion. It is shown that, for the collisionless neutrals, the neutral-gas density decreases as the neutral pressure increases. The neutral pressure is higher away from the wall, as it should be, resulting for collisionless neutrals in a lower density at the center of the discharge. This is in contrast to the case of the thermalized neutral gas studied in [32], the density and pressure of which are both larger away from the wall.

Manuscript received September 15, 2007; revised December 23, 2007. This work was supported in part by the Israel Science Foundation under Grant 864/07.

The author is with the Department of Sciences, H.I.T. - Holon Institute of Technology, Holon 58102, Israel (e-mail: fnfrucht@hit.ac.il).

Digital Object Identifier 10.1109/TPS.2008.918777

We distinguish between ion pumping [7]–[10], the neutral depletion described here, which follows neutrals becoming ions and leaving the discharge after being accelerated by the electric field, and neutral pumping. Neutral pumping is the process that we analyze in [34], in which neutrals in a collisional plasma leave the discharge after being accelerated toward the boundaries through charge-exchange collisions with fast ions. We note that the term "neutral pumping" has sometimes been used to describe what we call ion pumping.

For simplicity, we employ here a cold fluid model for the collisionless plasma ions, a model that is presented in Section II. It is shown that, as in the collisional case [29], the total number of neutrals determines the electron temperature. A general kinetic model for the neutrals is presented in Section III and applied to the case of a closed system of zero mass flow. The coupled plasma–neutral dynamics is solved in Section IV for the case of two counterpropagating cold neutral beams, which is the case that was also analyzed in [2]. In Section V, the asymptotic results for the cases of strong and weak neutral depletion are derived, and the profiles of neutral and plasma densities are presented for the two opposite limits. The relation between the neutral density and pressure is further exhibited in Section VI, unfolding the cause of depletion versus repletion.

An open system with a net mass flow is analyzed in Section VII. This analysis has relevance to plasma sources such as helicons that are considered for use as thrusters [35]–[44]. The analysis enables us to determine the densities and fluxes of both plasma and neutral particles along the channel. It is shown in Section VIII that, because of the presence of the sheath, the power flow into the backwall is larger than the power flow along the plasma exiting the source. The calculated profiles of the plasma and neutral particles along the channel are used in Section IX to derive expressions for the thrust, propellant utilization, specific impulse, and efficiency of a plasma source used as a thruster. The energy cost for ionization and the backwall energy losses are shown to significantly reduce the efficiency.

We start in the next section with the model for the collisionless plasma.

II. Model

Whereas in our previous study, we addressed the effect of neutral depletion on a plasma that is in a pressure balance with the neutral gas [29], here, we assume a collisionless plasma that is coupled to the neutrals through volume ionization and wall recombination only. Although such plasma ions can be kinetically analyzed [32], for simplicity, we employ a cold fluid model for the ions. The collisionless plasma is assumed quasi-neutral and 1-D, where all variables vary along z only. The electron and ion momentum equations, respectively, are the following:

$$\frac{d(nT)}{dz} = -neE \tag{1}$$

$$\frac{d(mnv^2)}{dz} - neE = -\nu_{ml} nv + m\beta nNV. \tag{2}$$

Here, n is the density of the quasi-neutral plasma, T is the (assumed constant) electron temperature, e is the elementary charge, E is the intensity of the ambipolar axial electric field, m and v are the mass and velocity of the ions, respectively, and N and V are the density and velocity of the neutrals, respectively. In (2), $\beta = \beta(T) \equiv \langle \sigma v_f \rangle$, where σ is the ionization cross section and the notation $\langle\rangle$ represents averaging over the distribution function of v_f, which is the electron velocity. The first term on the right-hand side (RHS) of the momentum equation expresses momentum losses in the z (axial) direction by ions that collide with lateral walls, to which z is parallel, and ν_{ml} is the coefficient of these momentum losses. We now make the approximation of neglecting the two terms on the RHS of this equation. The ions colliding with lateral walls are mostly the axially slower ions. Therefore, even if particle losses at the wall are not negligible, the momentum loss is small, making ν_{ml} small. Thus, for simplicity, we neglect this first term on the RHS. The second term is neglected because we assume that

$$V \ll v.$$

The sum of (1) and (2) becomes

$$\frac{d(mnv^2 + nT)}{dz} = 0 \tag{3}$$

expressing momentum conservation

$$mnv^2 + nT = n_0 T \tag{4}$$

where n_0 is the maximal plasma density.

By defining the plasma flux density

$$\Gamma = nv \tag{5}$$

we write (4) as

$$\Gamma^2/c^2 + n^2 = nn_0 \tag{6}$$

in which $c \equiv \sqrt{T/m}$ is the ion acoustic velocity. The plasma density is then expressed as

$$n = \left(\frac{n_0 + \sqrt{n_0^2 - 4\Gamma^2/c^2}}{2} \right). \tag{7}$$

The second solution of (6) for n corresponds to an unphysical plasma flow in which the plasma velocity v becomes infinite as Γ and n go to zero. From (7), we see that at the sheath edge of the plasma boundary

$$n_{\rm sheath} = n_{\rm min} = \frac{n_0}{2} \quad \Gamma_{\rm sheath} = \Gamma_{\rm max} = \frac{n_0}{2}c \quad v_{\rm max} = c. \tag{8}$$

A kinetic picture would give somewhat different and more accurate values of the parameters at the sheath edge. Note that these boundary conditions are independent of the value of N and are not affected by neutral depletion.

The deposited power per unit area of the plasma P equals the plasma-particle flux density to the wall $n_0 c/2$ multiplied by the energy deposited in each particle (or ion–electron pair) $\varepsilon_T = \varepsilon_T(T)$ [26]

$$P = \frac{n_0 c}{2} \varepsilon_T. \tag{9}$$

Note that the peak plasma density is determined by the electron temperature (through ε_T and c) and by the power density P and that it is also unaffected by neutral depletion.

For a collisional plasma, there is a coupling between the plasma and the neutral-gas pressures [29]. Here, as in [32], in which a kinetic treatment was employed, the plasma momentum is decoupled from the neutral pressure. The coupling inside the discharge between the plasma and the neutral gas is only through ionization as expressed in

$$\frac{d\Gamma}{dz} = \beta N n - \nu n. \tag{10}$$

The second term on the RHS of the equation represents particle losses at lateral walls, to which z is parallel. For an annular cross section, an approximate expression for these wall losses is $\nu = 2c/(r_{\rm out} - r_{\rm in})$, where $r_{\rm out}$ and $r_{\rm in}$ are the outer and inner channel radii, respectively, whereas, for a rectangular cross section, an approximate expression is $\nu = 2c(1/d_1 + 1/d_2)$, where d_1 and d_2 are the lengths of the two sides of the cross section. For now, we retain particle wall losses despite the neglect of momentum wall losses that are relatively smaller.

Equations (5), (7), and (10) can be combined to a differential equation for either Γ

$$\frac{d\Gamma}{dz} = (\beta N - \nu)\left(\frac{n_0 + \sqrt{n_0^2 - 4\Gamma^2/c^2}}{2}\right) \tag{11}$$

M

$$(1 - M^2)\frac{dM}{dz} = \frac{(\beta N - \nu)}{c}(M^2 + 1) \tag{12}$$

or n

$$\left(\frac{n_0}{n} - 2\right)\frac{dn}{dz} = 2\frac{(\beta N - \nu)}{c} n\sqrt{\frac{n_0}{n} - 1} \tag{13}$$

where $M \equiv v/c$ is the Mach number. Note the singularity at the sonic plane in (12).

Let us assume that the walls are located at $z = \pm a$. Then, integrating the aforementioned equations from $z = -a$ yields

$$\begin{aligned}
&\arcsin\Gamma_n - \frac{\Gamma_n}{\sqrt{1-\Gamma_n^2}+1} + \frac{\pi}{2} - 1 \\
&\quad = 2\arctan M + \frac{\pi}{2} - M - 1 \\
&\quad = 2\arcsin\left(1 - 2\frac{n}{n_0}\right) - \frac{2n_0}{n}\sqrt{\frac{n}{n_0}\left(1 - \frac{n}{n_0}\right)} + 2 \\
&\quad = \frac{\beta}{c}\int_{-a}^{z} N dz' - \frac{\nu}{c}(z + a)
\end{aligned} \tag{14}$$

where $\Gamma_n \equiv 2\Gamma/n_0 c$ and $\Gamma_n(z = \pm a) = \pm 1$. By substituting $\Gamma_n(z = a) = 1$, we obtain

$$\pi - 2 + s = \frac{\beta}{c}\int_{-a}^{a} N dz' = \frac{\beta}{c} N_T. \tag{15}$$

Here, $s = 2a\nu/c = 4a/(r_{\rm out} - r_{\rm in})$ or $s = 4(a/d_1 + a/d_2)$, which is a number determined by the geometry. Equations (14) and (15) are generalizations of the case of weakly ionized plasma to the case of a nonuniform neutral density induced by high ionization. In particular, (15) shows that, as in the pressure-balance case [29], the total number of neutrals per unit area N_T replaces the Paschen parameter of the weakly ionized plasma as the parameter that determines the electron temperature (through the determination of β/c).

We address here two cases of interest. The first case is of a closed system in which the mass-flow rate is zero, whereas the second case is of an open system with a net mass flow. We first describe a general formalism for the neutral dynamics.

III. Neutral Dynamics—No Mass Flow

We assume that the neutrals, like the plasma ions, are collisionless, that they move ballistically, and that they are coupled to the plasma only through volume ionization and wall recombination. The neutral dynamics under these assumptions has also been considered in [2]–[5], [14], and [16]. The neutral dynamics assumed here is different from that of the thermalized neutrals in that part in [32] in which the plasma was assumed collisionless. We assume that neutrals are reflected, and plasma recombines upon collisions with walls that are normal to z (at the axial boundaries of the discharge) only. Lateral wall losses are neglected. This is justified for a helicon source that employs a strong-enough magnetic field or for a wide-enough plasma source. The neutral-gas distribution function $f_N(v, z)$ is obtained by solving the following steady-state Boltzmann equation:

$$\frac{d(v f_N)}{dz} = -\beta n f_N \tag{16}$$

and is found to be

$$f_N(v, z) = f_N(v, -a)\exp\left[-\frac{\beta}{v}\int_{-a}^{z} n(z')dz'\right]. \tag{17}$$

For a closed system, we assume that the distribution function satisfies

$$f_N(v, z) = f_N(-v, -z), \qquad -a \le z \le a \tag{18}$$

so that

$$f_N(-v, -a) = f_N(v, -a)\exp\left(-2\frac{\beta}{v}\int_{-a}^{0} n(z')dz'\right). \tag{19}$$

The flow and the electric potential turn out to be symmetrical with respect to $z = 0$. From (18), the neutral density becomes

$$\begin{aligned}
N(z) = \int_0^\infty dv f_N(v, -a)\Bigg[&\exp\left(-\frac{\beta}{v}\int_{-a}^{z} n(z')dz'\right) \\
&+ \exp\left(-\frac{\beta}{v}\int_{z}^{a} n(z')dz'\right)\Bigg].
\end{aligned} \tag{20}$$

We note that, for every form of $f_N(v,-a)$, the neutral density decreases away from the wall. This is easily seen by examining the derivative of the density

$$\frac{dN(z)}{dz}=\beta(T)n(z)\int_0^\infty dv\frac{f_N(v,-a)}{v}\times\left[-\exp\left(-\frac{\beta}{v}\int_{-a}^{z}n(z')dz'\right)+\exp\left(-\frac{\beta}{v}\int_{z}^{a}n(z')dz'\right)\right]. \tag{21}$$

Because in the symmetrical discharge $\int_{-a}^{z}n(z')dz'\lessgtr\int_{z}^{a}n(z')dz'$ when $\mp a\lessgtr z\lessgtr 0$, the term in the square brackets is negative when $-a\le z<0$ and positive when $0<z\le a$. As a result

$$\frac{dN(z)}{dz}<0,\qquad -a\le z<0$$
$$\frac{dN(z)}{dz}>0,\qquad 0<z\le a. \tag{22}$$

Thus, collisionless neutrals that ballistically move between the walls will **always** have lower densities away from the walls, independent of their distribution function at the wall. As we already noted, this density profile is opposite in its shape to the density profile of the thermalized neutral gas analyzed in [32], in which the density maximum is at the center of the discharge, away from the walls. In both cases, the pressure of the neutral gas is higher at the center and lower near the walls. For the collisionless neutrals analyzed in this paper, the pressure has a maximum where the density has its minimum, which is at the center of the discharge. This difference between collisionless and thermalized neutral gas will be discussed further in Section VI.

We define the rate of neutral depletion as

$$D\equiv\frac{N(-a)-N(0)}{N(0)}=\frac{\int_0^\infty dvf_N(v,-a)\left[1-\exp\left(-\frac{\beta}{v}\int_{-a}^{0}n(z')dz'\right)\right]^2}{2\int_0^\infty dvf_N(v,-a)\left[\exp\left(-\frac{\beta}{v}\int_{-a}^{0}n(z')dz'\right)\right]}. \tag{23}$$

In Section V, asymptotic expressions will be derived for D, which is the rate of neutral depletion.

The neutral flux $\Gamma_N(z)$ is expressed as

$$\Gamma_N(z)=\int_0^\infty dvvf_N(v,-a)\left[\exp\left(-\frac{\beta}{v}\int_{-a}^{z}n(z')dz'\right)-\exp\left(-\frac{\beta}{v}\int_{z}^{a}n(z')dz'\right)\right]. \tag{24}$$

The total mass flux is zero

$$\Gamma(z)+\Gamma_N(z)=0. \tag{25}$$

By employing (6) and (24) for the plasma and neutral fluxes and by employing

$$g(z)\equiv\int_{-a}^{z}n(z')dz',\qquad n(z)=\frac{dg(z)}{dz} \tag{26}$$

we obtain a first-order differential equation for $g(z)$

$$c\sqrt{\frac{dg}{dz}n_0-\left(\frac{dg}{dz}\right)^2}+\int_0^\infty dvvf_N(v,-a)\times\left[\exp\left(-\frac{\beta}{v}g(z)\right)-\exp\left(-\frac{\beta}{v}g(a)+\frac{\beta}{v}g(z)\right)\right]=0. \tag{27}$$

Here, we do not solve this last general equation. Rather, in the next section, we will analyze the case in which the incoming neutrals are cold beams of a uniform velocity.

IV. Two Counterpropagating Cold Neutral Beams

Similar to what we did in [31] and to the analysis in [2], we choose, for simplicity, a velocity distribution function for the neutrals of the form

$$f_N(v,-a)=\frac{\Gamma_w}{v_a}\delta(v-v_a)+\frac{\Gamma_w}{v_a}\delta(v+v_a)\times\exp\left(-2\frac{\beta}{v}\int_{-a}^{a}n(z')dz'\right). \tag{28}$$

All ions are assumed to have a velocity of the same magnitude v_a in a direction that is either to the right or left. Here, Γ_w is the neutral flux density from the wall. We note that, as we have shown in Section III, depletion rather than repletion should occur for every distribution function of neutrals $f_N(v,-a)$ at the wall. The neutral-gas flux is written as

$$\Gamma_N(z)=\Gamma_1(z)-\Gamma_2(z) \tag{29}$$

which is composed of a flux to the right $\Gamma_1(z)$ and a flux to the left $\Gamma_2(z)$ of the forms

$$\Gamma_1(z)\equiv\Gamma_w\exp\left(-\frac{\beta}{v_a}\int_{-a}^{z}n(z')dz'\right)$$
$$\Gamma_2(z)\equiv\Gamma_w\exp\left(-\frac{\beta}{v_a}\int_{z}^{a}n(z')dz'\right). \tag{30}$$

The neutral-gas density is expressed as

$$N(z)=\frac{\Gamma_1(z)+\Gamma_2(z)}{v_a} \tag{31}$$

or

$$N=\frac{\sqrt{\Gamma^2(z)+4\Gamma_0^2}}{v_a}=\frac{\Gamma_{\max}}{v_a}\sqrt{\Gamma_n^2+B^2},\qquad B\equiv\frac{2\Gamma_0}{\Gamma_{\max}}. \tag{32}$$

The neutral depletion (23) is expressed here as

$$D \equiv \frac{N(\pm a) - N(0)}{N(0)} = \frac{\left[1 - \exp\left(-\frac{\beta}{v_a}\int\limits_{-a}^{0} n(z')dz'\right)\right]^2}{2\exp\left(-\frac{\beta}{v_a}\int\limits_{-a}^{0} n(z')dz'\right)} \quad (33)$$

and further as

$$D \equiv \frac{N(\pm a) - N(0)}{N(0)} = \sqrt{1 + \frac{1}{B^2}} - 1. \quad (34)$$

The neutral depletion is large when B is small.

By combining (25) and (29), we obtain

$$\Gamma + \Gamma_1 - \Gamma_2 = 0. \quad (35)$$

From (30), we derive the following relation between $\Gamma_1(z)$ and $\Gamma_2(z)$:

$$\Gamma_1(z)\Gamma_2(z) = \Gamma_w^2 \exp\left(-\frac{\beta}{v_a}\int\limits_{-a}^{a} n(z')dz'\right) = \Gamma_0^2$$
$$\Gamma_0 \equiv \Gamma_1(0) = \Gamma_2(0). \quad (36)$$

By substituting (32) for N into (11), in which, as we previously said that we neglect lateral wall losses ($\nu = 0$), we obtain

$$\frac{d\Gamma_n}{d\xi} = \frac{P_n}{2}\sqrt{\Gamma_n^2 + B^2}\left(1 + \sqrt{1 - \Gamma_n^2}\right) \quad (37)$$

where

$$\xi \equiv \frac{z}{a}; \qquad P_n \equiv \frac{\beta a n_0}{v_a}. \quad (38)$$

We can employ (9) to express n_0 with the deposited power P

$$P_n \equiv \frac{(2\pi - 1)aP}{N_T v_a \varepsilon_T} \qquad B \equiv \frac{2\varepsilon_T \Gamma_0}{P}. \quad (39)$$

In this form, P_n denotes normalized power. As P_n increases, B decreases, and D, which is the neutral depletion, increases.

V. Small and Large Neutral Depletion—No Mass Flow

In this section, we present asymptotic results and numerical examples. By integrating (37) from $\xi = 0$ to $\xi = 1$ at which $\Gamma_n = 1$, we obtain a relation between P_n and B

$$\int\limits_0^1 \frac{d\Gamma_n}{\sqrt{\Gamma_n^2 + B^2}\left(1 + \sqrt{1 - \Gamma_n^2}\right)} = \frac{P_n}{2}. \quad (40)$$

Let us find this relation at asymptotic limits. We start with the case of low depletion, occurring for $B \gg 1$. We then recover the weakly ionized case [(14) and (15), in which the neutral density N is assumed uniform]. The condition for low neutral depletion is as follows:

$$P_n \cong \frac{(\pi - 2)}{B} \ll 1 \Longrightarrow P \ll N v_a \varepsilon_T. \quad (41)$$

The more interesting case is of strong neutral depletion, when $B \ll 1$. Integral equation (40) is estimated as follows. Let us choose b such that $B \ll b \ll 1$ and split the integral into two, one in the interval $[0, b]$ and another in the interval $[b, 1]$. In the first integral, we approximate $1 + \sqrt{1 - \Gamma_n^2} \cong 2$, which means that we assume that the plasma density is approximately uniform and takes its maximal value. Thus

$$\int\limits_0^b \frac{d\Gamma_n}{2\sqrt{\Gamma_n^2 + B^2}} = \frac{1}{2}\ln\left(\frac{b + \sqrt{B^2 + b^2}}{B}\right) \cong \ln\sqrt{\frac{2b}{B}}. \quad (42)$$

The second integral is approximated as

$$\int\limits_b^1 \frac{1}{\left(1 + \sqrt{1 - \Gamma_n^2}\right)\Gamma_n} d\Gamma_n$$
$$= -\frac{1}{2} - \frac{1}{4}\ln\frac{1 - \sqrt{1 - b^2}}{1 + \sqrt{1 - b^2}} + \frac{1}{2(1 + \sqrt{1 - b^2})}$$
$$\cong -\frac{1}{4} + \ln\sqrt{\frac{2}{b}}. \quad (43)$$

The sum of the two approximated integrals for $B \ll 1$ results in

$$\frac{P_n}{2} = \int\limits_0^1 \frac{d\Gamma_n}{\sqrt{\Gamma_n^2 + B^2}\left(1 + \sqrt{1 - \Gamma_n^2}\right)} \cong -\frac{1}{4} + \ln\frac{2}{\sqrt{B}}. \quad (44)$$

From (34), we find that $B \ll 1 \Longrightarrow D \cong 1/B$. We therefore conclude that when neutral depletion is large

$$B \cong 4\exp\left(-P_n - \frac{1}{2}\right), \quad D \cong \frac{1}{4}\exp\left(P_n + \frac{1}{2}\right) \quad P_n \gg 1. \quad (45)$$

This is the rate of neutral depletion as a function of the normalized power P_n for large power.

Here, we present two numerical examples for two different values of P_n. The value of B is found by solving (40). The normalized plasma flux density Γ_n as a function of ξ is obtained as a solution of (37). By employing (7) and (32), we obtain the normalized plasma $n_n \equiv n/n_0$ and neutral $N_n \equiv N/N(\pm a)$ densities as functions of Γ_n

$$n_n = \frac{1}{2}\left(1 + \sqrt{1 - \Gamma_n^2}\right) \quad N_n = \sqrt{\frac{\Gamma_n^2 + B^2}{1 + B^2}}. \quad (46)$$

These normalized plasma density n_n and neutral density N_n are shown in Fig. 1 when the neutral depletion is small and in Fig. 2 when the neutral depletion is large.

VI. Density and Pressure of the Neutral Gas

The neutral density in Figs. 1 and 2 has a minimum at the center of the discharge, in contrast to the neutral-density

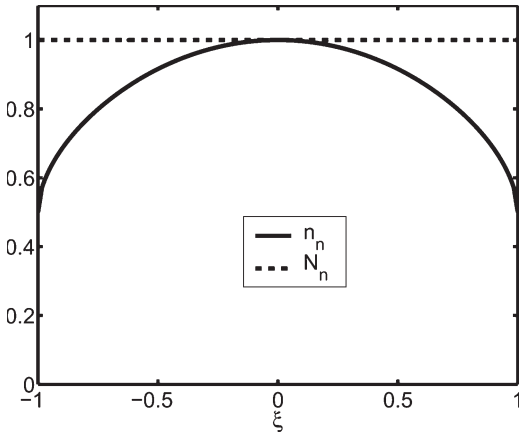

Fig. 1. Normalized plasma n_n and neutral N_n densities in the small depletion case, where $B^2 = 10^4$ and $P_n = 0.0114$.

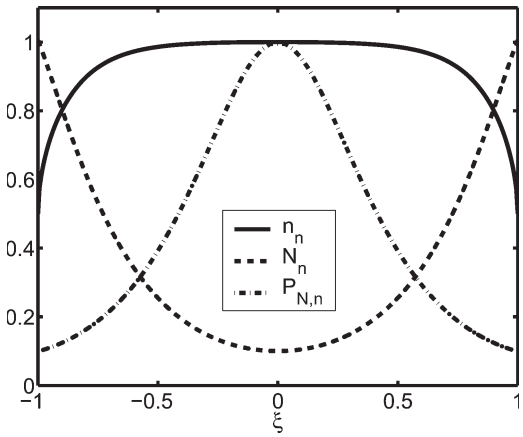

Fig. 2. Normalized plasma density n_n, neutral density N_n, and neutral pressure $P_{N,n}$ in the high depletion case, where $B^2 = 0.01$ and $P_n = 3.19$.

profile found in [32], which has a maximum at the center of the discharge. Here, we explain that difference. The continuity and the momentum equations for the neutrals obtained from (16) as

$$\frac{d(NV)}{dz} = -\beta N n \qquad \frac{d\left(mNV^2 + p_N\right)}{dz} = -m\beta N n V \tag{47}$$

are combined into

$$mNV\frac{dV}{dz} + \frac{dp_N}{dz} = 0. \tag{48}$$

The momentum equation in this form shows that, if the neutral flux points in the direction away from the wall and if the velocity decreases away from the wall, then the gas pressure should increase away from the wall. In the case in which $p_N = p_N(N)$, the neutral density profile is determined by

$$\frac{dp_N}{dz} = \frac{dp_N}{dN}\frac{dN}{dz}. \tag{49}$$

In [32], the neutrals were assumed to have the equation of state

$$p_N = NT_g \tag{50}$$

where T_g, which is the gas temperature, was assumed constant. Because

$$\frac{dp_N}{dN} = T_g > 0 \tag{51}$$

the spatial derivative of the neutral density has the same sign as the spatial derivative of the pressure. Thus, the neutral density, as the gas pressure, increases away from the wall

$$\frac{dp_N}{dz}\Big/\frac{dN}{dz} > 0. \tag{52}$$

For the neutrals of (28), however, the neutral-gas pressure satisfies

$$P_N(z) = m\left[N(z)v_a^2 - \frac{\Gamma_N^2(z)}{N(z)}\right] = \frac{4m\Gamma_0^2}{N(z)} \tag{53}$$

which is inversely proportional to the neutral density. As a result, the neutral density has its minimum where the neutral pressure has its maximum, which is at the center of the discharge. We have shown in Section III that depletion occurs for every distribution function of the neutrals at the wall. Therefore, the neutral density is lower where the neutral pressure is higher for every distribution function, although, the relation between neutral density and pressure generally cannot be written in as simple a manner as in (53).

By employing (53), we can relate the decrease of the neutral density at the center of the discharge associated with neutral depletion to the increase of neutral pressure

$$D \equiv \frac{N(\pm a)}{N(0)} - 1 = \frac{P_N(0)}{P_N(\pm a)} - 1. \tag{54}$$

We can express the normalized neutral pressure as

$$P_{N,n}(z) \equiv \frac{P_N(z)}{P_N(0)} = \frac{1}{\sqrt{1 + \Gamma_n^2/B^2}} \tag{55}$$

where $P_N(0) = 2mv_aB\Gamma_0$. In Fig. 2, the profile of the normalized neutral pressure $P_{N,n}(z)$ is shown. It is apparent that its maximum is at the center of the discharge.

VII. Plasma Source With a Net Mass-Flow Rate

In many systems of interest, there is a net mass flow. Neutrals are injected at one end of the system, and a mixture of neutral and ionized gases flows out of the system at the other end. The rate of ionization is important, because for various uses, it expresses the efficiency of a desired process. Helicon sources considered for propulsion are examples [35]–[44] of a system with a net mass flow. We present here an extension of the analysis in [30] of a system with a net mass flow. The implications of the possible presence of a double layer at the exit of the helicon source [35], [38], [42] or of a varying cross-section of the flow [37], [38], [41] are not discussed here.

We assume a neutral-gas distribution function at the gas inlet of the form

$$f_N(v) = N_0\delta(v - v_a) \tag{56}$$

where N_0 is the neutral density at the gas inlet upstream. We write the net mass-flow rate as

$$\Gamma + Nv_a = \Gamma_m \equiv \frac{\dot{m}}{Sm} \tag{57}$$

where Γ_m, which is the particle (neutral plus plasma) flux density, is expressed as the ratio of $\dot{m}$, which is the mass-flow rate, and the product of m and S, which is the channel cross section. Because we assume that v_a is uniform in the channel, (57) determines the value of the varying neutral density N along the channel as a function of the varying ion flux density Γ. The neutral density is therefore

$$N = \frac{1}{v_a}(\Gamma_m - \Gamma). \tag{58}$$

As we did in Section III, we neglect here the lateral wall losses, substituting $\nu = 0$ in (12). Equation (12), in which we use (58) and also the relation $\Gamma = n_0 cM/(M^2+1)$, becomes

$$(1-M^2)\frac{dM}{dz} = \frac{1}{\lambda_{\text{ion}}}\left(M^2 + 1 - 2\eta_m M\right) \tag{59}$$

where

$$\eta_m \equiv \frac{\Gamma\left(z_{\text{exit}}\right)}{\Gamma_m}; \quad \lambda_{\text{ion}} \equiv \frac{v_a c}{\beta \Gamma_m}. \tag{60}$$

Here, η_m is the propellant utilization and $\Gamma(z_{\text{exit}}) = \Gamma_{\max} = n_0 c/2$ is the ion flux density at the gas exit from the source. Also, λ_{ion} is a characteristic ionization mean free path of the plasma flow. The last equation can be integrated to

$$-1 - M - \eta_m \ln\left(\frac{M^2+1-2\eta_m M}{2+2\eta_m}\right) + 2\sqrt{1-\eta_m^2} \times \left[\arctan\left(\frac{M-\eta_m}{\sqrt{1-\eta_m^2}}\right) - \arctan\left(\frac{-1-\eta_m}{\sqrt{1-\eta_m^2}}\right)\right] = \frac{z}{\lambda_{\text{ion}}} \tag{61}$$

which satisfies $M = -1$ at $z = 0$. By requiring that $M = 1$ at $z = L \equiv z_{\text{exit}}$, we obtain

$$-2 - \eta_m \ln\left(\frac{1-\eta_m}{1+\eta_m}\right) + 2\sqrt{1-\eta_m^2} \times \left[\arctan\left(\frac{1-\eta_m}{\sqrt{1-\eta_m^2}}\right) - \arctan\left(\frac{-1-\eta_m}{\sqrt{1-\eta_m^2}}\right)\right] = \frac{L}{\lambda_{\text{ion}}}. \tag{62}$$

The propellant utilization is determined by L/λ_{ion}, which is the number of ionization mean free paths along the channel. We can now write the profile of the ion flow velocity, shown at the bottom of the page.

We equivalently define the rate of neutral depletion to the previous case of no mass flow as

$$D \equiv \frac{N(z=0) - N(z=L)}{N(z=L)}. \tag{64}$$

Because $N(z=0)v_a = \dot{m}/Sm - \Gamma(0)$, $N(z=L)v_a = \dot{m}/Sm - \Gamma(L)$, and $\Gamma(0) = -\Gamma(L)$, we obtain

$$D = \frac{2\eta_m}{1-\eta_m}. \tag{65}$$

At the limit of low ionization, (62) yields

$$\pi - 2 = \frac{L}{\lambda_{\text{ion}}} = \frac{\beta N L}{c}, \qquad \eta_m \ll 1. \tag{66}$$

Here, N is the constant neutral density. At the opposite limit of large neutral depletion

$$\eta_m = 1 - 2\exp\left(-\frac{L}{\lambda_{\text{ion}}}\right), \qquad \frac{\lambda_{\text{ion}}}{L}, 1-\eta_m \ll 1. \tag{67}$$

From (65) and (67), the neutral depletion is then approximated as

$$D = \exp\left(\frac{L}{\lambda_{\text{ion}}}\right). \tag{68}$$

Fig. 3 shows the two cases of a net mass flow, one of a low ($\eta_m = 0.001$) neutral depletion and another of a high ($\eta_m = 0.999$) neutral depletion. Note that, although when neutral depletion is high, the plasma profiles are very asymmetrical, the plasma density and plasma flux density are identical on both sides of the channel. Fig. 4 shows the plasma and the neutral flux densities, both normalized to the particle flux density Γ_m, for these two cases. In the case of low propellant utilization, $\eta_m = 0.001$, the plasma flux is only a small fraction of the particle flux and the neutral flux is hardly modified. When neutral depletion is high, $\eta_m = 0.999$, the neutral flux is almost zero at the exit. At the inlet, because of the large plasma backflow, the neutral flux is approximately twice the particle flux.

VIII. Power Flow at a Plasma Boundary

Equation (9) determines the power deposited per unit area of the plasma boundary. The energy $\varepsilon_T(T)$ deposited in an ion–electron pair of the plasma flow into a sheath near a wall is different from that deposited in an ion–electron pair of the plasma flow at an open boundary. At a wall, that energy is expressed as [26]

$$\varepsilon_{Ts} = \varepsilon_c + 2T + 0.5T\left[1 + \ln\left(\frac{1}{2\pi}\frac{m}{m_e}\right)\right] \tag{69}$$

$$\frac{-1 - M - \eta_m \ln\left(\frac{M^2+1-2\eta_m M}{2+2\eta_m}\right) + 2\sqrt{1-\eta_m^2}\left[\arctan\left(\frac{M-\eta_m}{\sqrt{1-\eta_m^2}}\right) - \arctan\left(\frac{-1-\eta_m}{\sqrt{1-\eta_m^2}}\right)\right]}{-2 - \eta_m \ln\left(\frac{1-\eta_m}{1+\eta_m}\right) + 2\sqrt{1-\eta_m^2}\left[\arctan\left(\frac{1-\eta_m}{\sqrt{1-\eta_m^2}}\right) - \arctan\left(\frac{-1-\eta_m}{\sqrt{1-\eta_m^2}}\right)\right]} = \frac{z}{L} \tag{63}$$

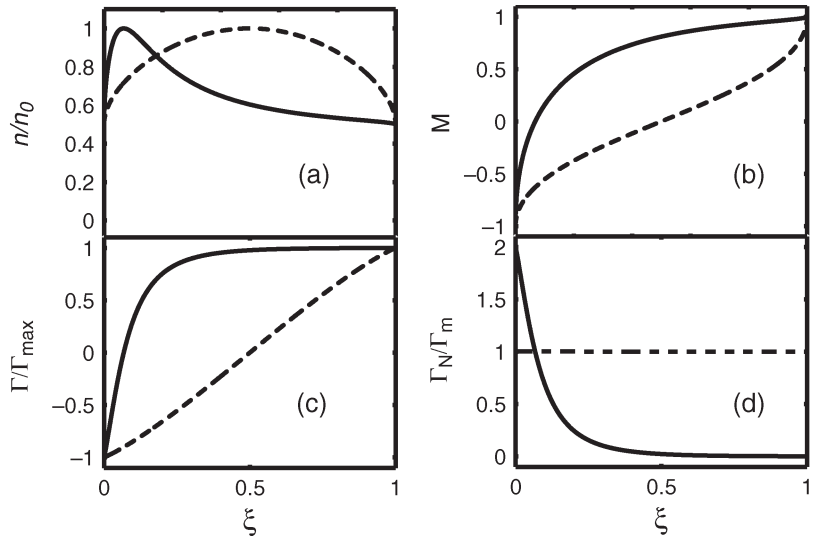

Fig. 3. Open system with a net mass-flow rate, where (dashed) $\eta_m = 0.001$ and (solid) $\eta_m = 0.999$. The gas inlet is on the left and the exit, which is the open boundary, is on the right. Shown are the profiles of (a) plasma density, (b) Mach number, (c) plasma flux density, and (d) neutral-gas flux density.

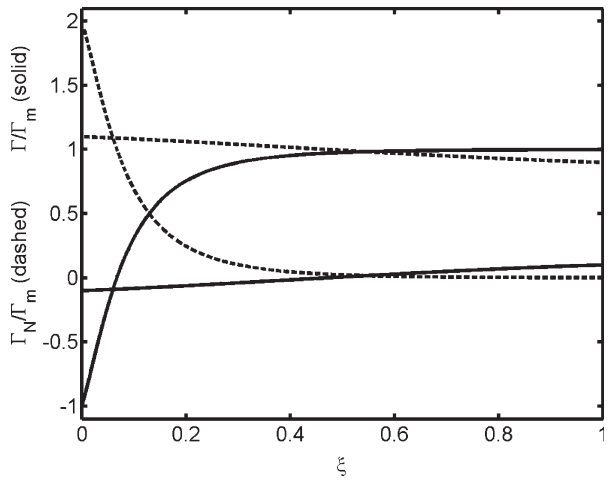

Fig. 4. Open system with a net mass-flow rate, where $\eta_m = 0.1$ and $\eta_m = 0.999$. Shown are the profiles of (solid) plasma and (dashed) neutral flux densities, both normalized to the particle flux density. The gas inlet is on the left and the exit, which is the open boundary, is on the right. When $\eta_m = 0.999$, the plasma flux density is larger and the variation of the neutral flux density is more apparent.

where m_e is the electron mass. The first term, which is ε_c, is the energy cost for ionization, $2T$ is the average energy flux for an electron, and the last term is the energy deposited in the ions, $0.5T$ in the presheath and the rest while they are accelerated in the sheath. The total energy deposited in an ion–electron pair that crosses the sonic plane at an open boundary, however, is written as

$$\varepsilon_{Te} = \varepsilon_c + 1.5T + 0.5T. \tag{70}$$

The first term is the same energy cost for ionization as in the expression for ε_{Ts}, the second term is the average thermal energy carried by an electron, and the third term is the kinetic energy of an ion $mc^2/2 = T/2$.

As we previously mentioned, we neglect particle and energy losses at lateral walls. There are losses at the two axial boundaries only, at the backwall, which is the gas inlet at one end, and at the open boundary, through which neutral and ionized gases exit the discharge at the other end. The power balance is therefore written as

$$P_T = \frac{n_0 c}{2} S(\varepsilon_{Ts} + \varepsilon_{Te}). \tag{71}$$

Here, P_T is the total power deposited in the plasma and $n_0 c/2 = \Gamma(0) = \Gamma(z_{\text{exit}})$ is the plasma flux density at each of the two boundaries. By using (71) to write the plasma flux density $\Gamma(z_{\text{exit}})$ as $P_T/[S(\varepsilon_{Ts} + \varepsilon_{Te})]$ in (60), we express the propellant utilization as

$$\eta_m = \frac{P_T}{(\varepsilon_{Ts} + \varepsilon_{Te})} \frac{m}{\dot{m}}. \tag{72}$$

Equation (72), the expression

$$\frac{L}{\lambda_{\text{ion}}} = \frac{\dot{m}\beta L}{m S v_a c} \tag{73}$$

that follows (60), and (67) result in the following relation that holds when the propellant utilization is high:

$$\frac{P_T}{(\varepsilon_{Ts} + \varepsilon_{Te})} \frac{m}{\dot{m}} \cong 1 - 2\exp\left(-\frac{\dot{m}\beta L}{m S v_a c}\right). \tag{74}$$

Generally, by specifying the total deposited power P_T and by substituting the expression for η_m from (72) and the expression for L/λ_{ion} from (73) into (62), we obtain a relation that determines the electron temperature T, once the dependencies of ε_c and β on T are specified.

IX. Plasma Thruster

There has recently been an interest in employing helicon-plasma sources for electric propulsion, either by themselves or as a plasma source with another acceleration mechanism added [35]–[44]. We discuss here the effects of particle and power balance on the performance of such a thruster.

The thrust of a plasma thruster of a uniform cross-section along the flow is as follows:

$$F = n_0 TS = \left(\frac{n_0}{2}T + m\frac{n_0}{2}c^2\right)S. \tag{75}$$

Note that this is the force that the plasma exerts on the backwall. The ions that impinge on the backwall exert a much larger force on it than that in (75). However, because of their positive charge, the ions in the sheath exert, on the negatively charged backwall, a large force in the **opposite** direction. The net momentum that the ions deliver to the backwall is a result of the difference between these opposing forces and equals the momentum flux that they carry upon entering the sheath at the presheath–sheath boundary. A similar momentum is also delivered to the backwall by the electrons in the sheath that are repelled by the negatively charged backwall. The net momentum delivered by the whole plasma, ions and electrons, is a result of the force [(75)], which is due to the maximal electron pressure. Thus, the additional larger momentum gained by the ions in the sheath and then lost during their collision with the wall does not contribute to the thrust; rather, it results in an energy loss only in the form of heat.

The momentum delivery can also be explained in terms of the electric force. The negatively charged backwall is **attracted** by the positively charged plasma in a direction that is opposite to the net thrust delivered. The momentum delivered by the ions while colliding with the wall balances that attractive electric force and provides, in addition, an extra thrust of a density that equals to the maximal electron pressure as expressed in (75). It is interesting to note that a neutral gas delivers momentum density to a wall that equals its pressure without those sheath losses in the form of heat.

The thrust can be also written as

$$F = 2c\eta_m \dot{m}. \tag{76}$$

By using that expression for the thrust, we write the specific impulse as

$$I_{\rm sp} \equiv \frac{F}{\dot{m}g} = \frac{2c\eta_m}{g} \tag{77}$$

where g is the free-fall acceleration. When all the thermal energy in the flow is converted into directed energy, the flow velocity is twice the sonic velocity, $v = 2c$.

By employing (71), we write the ratio of thrust to power as

$$\frac{F}{P_T} = \frac{2\sqrt{mT}}{(\varepsilon_{Ts} + \varepsilon_{Te})} \tag{78}$$

which is an expression that shows the advantage of employing a propellant of high atomic mass and low ε_c. The efficiency, which is defined as

$$\eta = \frac{F^2}{2\dot{m}P_T} \tag{79}$$

turns out to be

$$\eta = \frac{\eta_m}{\varepsilon_c/T + 2 + 0.25\left[1 + \ln(m/2\pi m_e)\right]}. \tag{80}$$

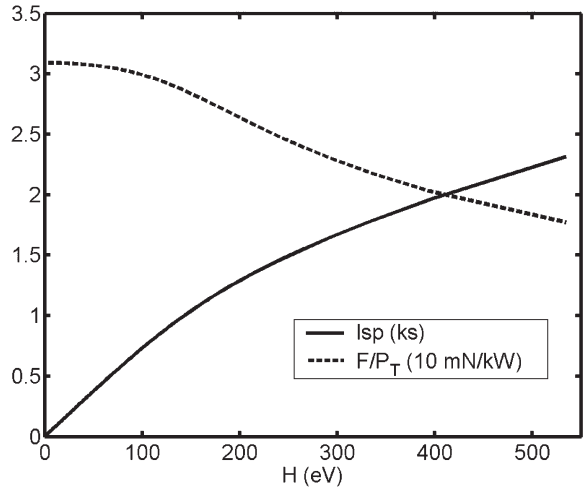

Fig. 5. Specific impulse and the ratio of thrust to power as a function of the power per particle. The propellant is argon, and $G = 4.14$.

From this expression, it is clear that the sheath potential significantly reduces the efficiency. The wall sheath is a sink of energy that does not contribute to the thrust. For high efficiency, a low ε_c is essential, as well as a high η_m. The difficulty of reaching a high efficiency is apparent from this expression.

We now numerically examine the effect of power on a thruster that uses a plasma source as previously analyzed. We use a simplified expression for the ionization rate

$$\beta = \sigma_0 v_{\rm te} \exp\left(-\frac{\epsilon_i}{T}\right) \tag{81}$$

where $v_{\rm te} \equiv (8T/\pi m_e)^{1/2}$ and $\sigma_0 \equiv \pi(e/4\pi\epsilon_0\epsilon_i)^2$, where ϵ_0 is the permittivity of the vacuum and ϵ_i is the ionization energy. We note that β/c reaches a limit as T is increased

$$\left(\frac{\beta}{c}\right)_{\max} = \sigma_0\sqrt{\frac{8m}{\pi m_e}} \text{ as } T \longrightarrow \infty$$

$$\Longrightarrow G \equiv \left(\frac{L}{\lambda_{\rm ion}}\right)_{\max} = \frac{\dot{m}L\sigma_0}{mSv_a}\sqrt{\frac{8m}{\pi m_e}}. \tag{82}$$

This maximal value determines the maximal propellant utilization η_m through (62). The expression in (82) that results in an upper bound on η_m shows that operating at a low mass-flow rate usually results in a low propellant utilization. It also explains the increase of the propellant utilization in a Hall thruster that was reached by extending the length of the channel [45]–[48]. Lateral wall losses were suggested to limit the possible advantage of a long channel [45]–[48], as has been theoretically shown in [30]. The effect of lateral wall losses will be examined in a subsequent study. The energy cost for ionization is approximated in our calculation as $\varepsilon_c(T) = \epsilon_i + \varepsilon_1 \exp[-6(T - T_1)/\epsilon_i]$.

We now assume that the gas is argon, so that $\epsilon_i = 15.76$ eV, and we use $\varepsilon_1 = 65$ eV, and $T_1 = 2$ eV. For argon, $G = (L/\lambda_{\rm ion})_{\max} = 1.71 \times 10^8(\dot{m}L/Sv_a)$ m$^2 \cdot$ kg^{-1}. For a specified value of G, we solve (62) for T as a function of H, where

$$H \equiv \frac{mP_T}{\dot{m}} \qquad \eta_m = \frac{H}{\varepsilon_{Ts} + \varepsilon_{Te}}. \tag{83}$$

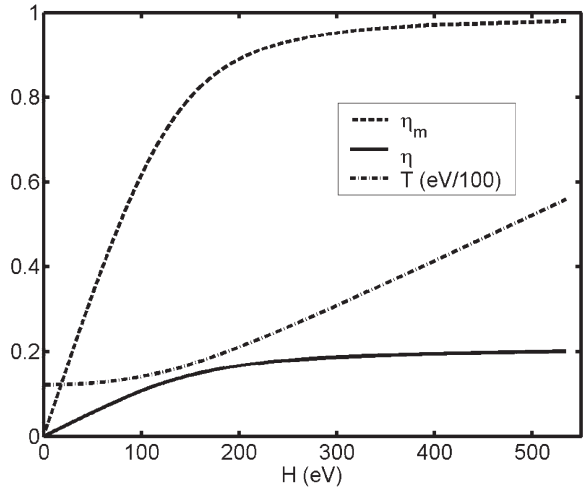

Fig. 6. Electron temperature, propellant utilization, and total efficiency as functions of the power per particle. The propellant is argon, and $G = 4.14$.

As an example, we choose $G = 4.14$, which corresponds to $\dot{m}L/Sv_a = 2.42 \times 10^{-8}\ \mathrm{m}^{-2} \cdot \mathrm{kg}$. In Fig. 5, shown are I_{sp} and F/P_T as functions of H. The specific impulse reaches 2300 s, and F/P_T decreases from 30 to 18 mN/kW with the power increase. In Fig. 6, shown are T, η_m, and η as functions of H. It is clear that the efficiency is inherently low and does not increase above 20%.

The total power is obtained as $P_T = (\dot{m}/m)H$, and the thrust is obtained as $F = (\dot{m}/m)H(F/P_T)$. For $S/L = 0.25$ m and $v_a = 500\ \mathrm{m} \cdot \mathrm{s}^{-1}$, the mass-flow rate is 3 $\mathrm{mg} \cdot \mathrm{s}^{-1}$. The power then reaches 3950 W, and the thrust reaches 72 mN.

X. Summary

In this paper, we have analyzed the effect of neutral depletion in a collisionless plasma interacting with a collisionless neutral gas. This analysis adds to our previous analyses of neutral depletion that occurs in plasma that is in pressure balance with neutrals [29] and of neutral depletion in collisionless plasma interacting with thermalized neutral gas [32]. The present analysis is relevant for various low-temperature plasmas generated in a low-pressure gas. The use of plasma sources as thrusters has also been discussed. The reduction of the energy cost for ionization and of the energy backwall losses was shown to be essential for increasing the efficiency. The effects of neutral depletion in the presence of neutral heating or of a magnetic field will be addressed in future studies.

Acknowledgment

The author would like to thank Prof. M. Lieberman, Prof. N. Hershkowitz, G. Makrinich, and Dr. B. Lane for the helpful comments.

References

[1] J. E. Allen and P. C. Thonemann, "Current limitation in the low-pressure mercury arc," *Proc. Phys. Soc. B*, vol. 67, no. 10, p. 768, Oct. 1954.

[2] A. Caruso and A. Cavaliere, "The low pressure discharge in the strong ionization regime," *Br. J. Appl. Phys.*, vol. 15, no. 9, pp. 1021–1029, Sep. 1964.

[3] P. C. Stangeby and J. E. Allen, "Current limitation in mercury vapour discharges—I. Theory," *J. Phys. A, Gen. Phys.*, vol. 4, no. 1, pp. 108–119, Jan. 1971.

[4] P. C. Stangeby and J. E. Allen, "Current limitation in mercury vapour discharges—II. Experiment," *J. Phys. D, Appl. Phys.*, vol. 6, no. 2, pp. 224–242, Jan. 1973.

[5] H. B. Valentini, "Theoretical description of gas discharges containing excited atoms at low pressures," *J. Phys. D, Appl. Phys.*, vol. 17, no. 5, pp. 931–951, May 1984.

[6] R. W. Boswell and K. Porteous, "Large volume, high density RF inductively coupled plasma," *Appl. Phys. Lett.*, vol. 50, no. 17, pp. 1130–1132, Apr. 1987.

[7] I. D. Sudit and F. F. Chen, "Discharge equilibrium of a helicon plasma," *Plasma Sources Sci. Technol.*, vol. 5, no. 1, pp. 43–53, 1996.

[8] J. Gilland, J. R. Breun, and N. Hershkowitz, "Neutral pumping in a helicon discharge," *Plasma Sources Sci. Technol.*, vol. 7, no. 3, pp. 416–422, Aug. 1998.

[9] A. W. Degeling, T. E. Sheridan, and R. W. Boswell, "Model for relaxation oscillations in a helicon discharge," *Phys. Plasmas*, vol. 6, no. 5, pp. 1641–1648, May 1999.

[10] A. W. Degeling, T. E. Sheridan, and R. W. Boswell, "Intense on-axis plasma production and associated relaxation oscillations in a large volume helicon source," *Phys. Plasmas*, vol. 6, no. 9, pp. 3664–3673, Sep. 1999.

[11] S. Yun, K. Taylor, and G. R. Tynan, "Measurement of radial neutral pressure and plasma density profiles in various plasma conditions in large-area high-density plasma sources," *Phys. Plasmas*, vol. 7, no. 8, pp. 3448–3456, Aug. 2000.

[12] E. J. Tonnis and D. B. Graves, "Neutral gas temperatures measured within a high-density, inductively coupled plasma abatement device," *J. Vac. Sci. Technol. A, Vac. Surf. Films*, vol. 20, no. 5, pp. 1787–1795, Sep. 2002.

[13] H. Abada, P. Chabert, J. P. Booth, J. Robiche, and G. Gartry, "Gas temperature gradients in a CF_4 inductive discharge," *J. Appl. Phys.*, vol. 92, no. 8, pp. 4223–4230, Oct. 2002.

[14] C. Watts and J. Hanna, "Alfvén wave propagation in a partially ionized plasma," *Phys. Plasmas*, vol. 11, no. 4, pp. 1358–1365, Apr. 2004.

[15] B. Clarenbach, M. Krämer, and B. Lorenz, "Spectroscopic investigations of electron heating in a high-density helicon discharge," *J. Phys. D, Appl. Phys.*, vol. 40, no. 17, pp. 5117–5129, Sep. 2007.

[16] J. E. Maggs, T. A. Carter, and R. J. Taylor, "Transition from Bohm to classical diffusion due to edge rotation of a cylindrical plasma," *Phys. Plasmas*, vol. 14, no. 5, 052 507, May 2007.

[17] M. Shimada, G. R. Tynan, and R. Cattolica, "Neutral gas density depletion due to neutral gas heating and pressure balance in an inductively coupled plasma," *Plasma Sources Sci. Technol.*, vol. 16, no. 1, pp. 193–199, Feb. 2007.

[18] A. M. Keesee and E. E. Scime, "Neutral argon density profile determination by comparison of spectroscopic measurements and a collisional-radiative model," *Rev. Sci. Instrum.*, vol. 77, no. 10, 10F304, Oct. 2006.

[19] A. M. Keesee and E. E. Scime, "Neutral density profiles in argon helicon plasmas," *Plasma Sources Sci. Technol.*, vol. 16, no. 1, pp. 742–749, Nov. 2007.

[20] A. Aanesland, L. Liard, G. Leray, J. Jolly, and P. Chabert, "Direct measurements of neutral density depletion by two-photon absorption laser-induced fluorescence spectroscopy," *Appl. Phys. Lett.*, vol. 91, no. 12, 121 502, Sep. 2007.

[21] D. O'Connell, T. Gans, D. L. Crintea, U. Czarnetzki, and N. Sadeghi, "Neutral gas depletion mechanisms in dense low-temperature argon plasmas," *J. Phys. D, Appl. Phys.*, vol. 41, no. 3, p. 035 208, Feb. 2008.

[22] W. Schottky, *Phys. Z.*, vol. 25, p. 635, 1924.

[23] J. R. Forrest and R. N. Franklin, "The positive column in a magnetic field at low pressures: The transition from free-fall to ambipolar conditions," *Br. J. Appl. Phys.*, vol. 17, no. 12, pp. 1569–1574, Dec. 1966.

[24] R. N. Franklin, *Plasma Phenomena in Gas Discharges*. Oxford, U.K.: Clarendon, 1976.

[25] V. A. Godyak, *Soviet Radio Frequency Discharge Research*. Falls Church, VA: Delphic Associates, 1986.

[26] M. A. Lieberman and A. J. Lichtenberg, *Principles of Plasma Discharges and Materials Processing*. New York: Wiley, 1994.

[27] A. Fruchtman, G. Makrinich, and J. Ashkenazy, "Two-dimensional equilibrium of a low temperature magnetized plasma," *Plasma Sources Sci. Technol.*, vol. 14, no. 1, pp. 152–167, Feb. 2005.

[28] N. Sternberg, V. Godyak, and D. Hoffman, "Magnetic field effects on gas discharge plasmas," *Phys. Plasmas*, vol. 13, no. 6, 063 511, Jun. 2006.

[29] A. Fruchtman, G. Makrinich, P. Chabert, and J. M. Rax, "Enhanced plasma transport due to neutral depletion," *Phys. Rev. Lett.*, vol. 95, no. 11, 115 002, Sep. 2005.

[30] A. Fruchtman, "The effect of the magnetic field profile on the plume and on the plasma flow in the Hall thruster," presented at the 29th Int. Electric Propulsion Conf., Princeton, NJ, 2005, IEPC Paper No. 2005-068.
[31] A. Fruchtman, "Neutral depletion and pressure balance in plasma," presented at the 33rd Eur. Physical Society Conf. Plasma Physics, vol. 30I, Rome, Italy, 2006, Paper No. D-5.013.
[32] J.-L. Raimbault, L. Liard, J.-M. Rax, P. Chabert, A. Fruchtman, and G. Makrinich, "Steady-state isothermal bounded plasma with neutral dynamics," *Phys. Plasmas*, vol. 14, no. 1, 013 503, Jan. 2007.
[33] L. Liard, J.-L. Raimbault, J.-M. Rax, and P. Chabert, "Plasma transport under neutral gas depletion conditions," *J. Phys. D, Appl. Phys.*, vol. 40, no. 17, pp. 5192–5195, Sep. 2007.
[34] A. Fruchtman, "Energizing and depletion of neutrals by a collisional plasma," *Plasma Sources Sci. Technol*. submitted for publication.
[35] C. Charles, "A review of recent laboratory double layer experiments," *Plasma Sources Sci. Technol.*, vol. 16, no. 4, pp. R1–R25, Nov. 2007.
[36] F. F. Chang-Diaz, "The Vasimir rocket," *Sci. Amer.*, vol. 283, p. 90, 2000.
[37] W. M. Manheimer and R. F. Fernsler, "Plasma acceleration by area expansion," *IEEE Trans. Plasma Sci.*, vol. 29, no. 1, pp. 75–84, Feb. 2001.
[38] A. Fruchtman, "Electric field in a double layer and the imparted momentum," *Phys. Rev. Lett.*, vol. 96, no. 6, p. 065 002, Feb. 2006.
[39] A. Dunaevsky, Y. Raitses, and N. J. Fisch, "Plasma acceleration from radio-frequency discharge in dielectric capillary," *Appl. Phys. Lett.*, vol. 88, no. 25, 251 502, Jun. 2006.
[40] F. F. Chen, "Permanent magnet helicon source for ion propulsion," *IEEE Trans. Plasma Sci.*, 2007. submitted for publication.
[41] R. Winglee, T. Ziemba, L. Giersch, J. Prager, J. Carscadden, and B. R. Roberson, "Simulation and laboratory validation of magnetic nozzle effects for the high power helicon thruster," *Phys. Plasmas*, vol. 14, no. 6, 063 501, Jun. 2007.
[42] M. Manente, J. Carlsson, I. Musso, C. Bramanti, D. Pavarin, and F. Angrilli, "Numerical simulation of the Helicon double layer thruster concept," presented at the 43rd Joint Propulsion Conf., Cincinnati, OH, Jul. 2007, AIAA Paper No. 2007-5312.
[43] O. Batishchev, N. Sinenian, M. Celik, and M. Martinez-Sanchez, "Development of the mini-helicon thruster at MIT," presented at the 30th Int. Electric Propulsion Conf., Florence, Italy, 2007, IEPC Paper No. 2007- 355.
[44] D. Palmer, C. Akinli, L. Williams, and M. L. R. Walker, "Characterization of an annular helicon plasma source," presented at the 30th Int. Electric Propulsion Conf., Florence, Italy, 2007, IEPC Paper No. 2007- 202.
[45] Y. Raitses, J. Ashkenazy, and M. Guelman, "Propellant utilization in Hall thrusters," presented at the 32nd Joint Propulsion Conf., Lake Buena Vista, FL, Jul. 1996, AIAA Paper No. 96-3193.
[46] K. Komurasaki, K. Mikami, and D. Kusamoto, "Channel length and thruster performance of Hall thrusters," presented at the 32nd Joint Propulsion Conf., Lake Buena Vista, FL, Jul. 1996, AIAA Paper No. 96-3194.
[47] Y. Raitses, J. Ashkenazy, and M. Guelman, "Propellant utilization in Hall thrusters," *J. Propuls. Power*, vol. 14, no. 2, pp. 247–253, 1998.
[48] J. Ashkenazy, Y. Raitses, and G. Appelbaum, "Parametric studies of the hall current plasma thruster," *Phys. Plasmas*, vol. 5, no. 5, pp. 2055–2063, May 1998.

Amnon Fruchtman (M'00) was born in Rehovot, Israel. He received the B.Sc. degree in physics from Tel Aviv University, Tel Aviv, Israel, in 1973, and the M.Sc. and Ph.D. degrees in physics from the Hebrew University of Jerusalem, Jerusalem, Israel, in 1976 and 1983, respectively.

After being a Postdoctoral Fellow with the Courant Institute of Mathematical Sciences, New York University, New York, he joined the Weizmann Institute of Science, Rehovot, which he left as an Associate Professor in 1995. He is now a Professor with the Department of Sciences, Holon Institute of Technology, Holon, Israel. He spent sabbaticals with Princeton University, Princeton, NJ, from 1994 to 1995 and with Ecole Polytechnique, Paris, France, in 2004. His areas of interest are free electron lasers, high-power pulsed plasmas, helicon and other plasma sources, and electric propulsion.

Prof. Fruchtman is a Fellow of the American Physical Society.